Modeling angular-dependent spectral emissivity of snow and ice in the thermal infrared atmospheric window

Masahiro Hori,[1,*] Teruo Aoki,[2] Tomonori Tanikawa,[1] Akihiro Hachikubo,[3] Konosuke Sugiura,[4] Katsuyuki Kuchiki,[2] and Masashi Niwano[2]

[1]Earth Observation Research Center, Japan Aerospace Exploration Agency, 2-1-1, Sengen, Tsukuba, Ibaraki 305-8505, Japan

[2]Meteorological Research Institute, 1-1 Nagamine, Tsukuba, Ibaraki 305-0052, Japan

[3]Environmental and Energy Resources Research Center, Kitami Institute of Technology, 165 Koen-cho, Kitami 090-8507, Japan

[4]Center for Far Eastern Studies, University of Toyama, 3190, Gofuku, Toyama-shi, Toyama 930-8555, Japan

*Corresponding author: hori.masahiro@jaxa.jp

Received 20 May 2013; revised 7 August 2013; accepted 16 September 2013; posted 17 September 2013 (Doc. ID 190829); published 15 October 2013

A model of angular-dependent emissivity spectra of snow and ice in the 8–14 μm atmospheric window is constructed. Past field research revealed that snow emissivity varies depending on snow grain size and the exitance angle. Thermography images acquired in this study further revealed that not only welded snow particles such as sun crust, but also disaggregated particles such as granular snow and dendrite crystals exhibit high reflectivity on their crystal facets, even when the bulk snow surface exhibits blackbody-like behavior as a whole. The observed thermal emissive behaviors of snow particles suggest that emissivity of the bulk snow surface can be expressed by a weighted sum of two emissivity components: those of the specular and blackbody surfaces. Based on this assumption, a semi-empirical emissivity model was constructed; it is expressed by a linear combination of specular and blackbody surfaces' emissivities with a weighting parameter characterizing the specularity of the bulk surface. Emissivity spectra calculated using the model succeeded in reproducing the past *in situ* measured directional spectra of various snow types by employing a specific weighting parameter for each snow type.

OCIS codes: (280.0280) Remote sensing and sensors; (280.6780) Temperature; (290.0290) Scattering; (290.6815) Thermal emission.

http://dx.doi.org/10.1364/AO.52.007243

1. Introduction

Directional emissivity spectra of snow cover at thermal infrared (TIR) wavelengths are essential properties for remote sensing of the earth's thermal properties, such as snow surface temperature [1–5], cloud discrimination from space [6,7], and for estimating Earth's long-wave radiation budget on the Greenland and Antarctic ice sheets by broadband radiometer such as the clouds and the Earth's radiant energy system (CeRES) [8]. The spectra may also be potentially utilized for sensing remote planets in astronomical applications [9].

The spectral emissivities of snow in TIR had been investigated based on theoretical radiative transfer (RT) calculation approaches in addition to laboratory or field measurements. Berger [10] indicated that

1559-128X/13/307243-13$15.00/0

snow emissivity exhibits weak dependence on snow density by adapting a simple geometric optics approximation to the theoretical scattering calculation. Dozier and Warren [11] simulated the directional-hemispherical reflectance (DHR) of snow, which can be equalized to $1 - \varepsilon$ using Kirchhoff's law (where ε is the directional emissivity at an exitance angle), based on a more rigorous treatment: Mie scattering for single scattering and the delta-Eddington approximation for multiple scattering. This indicated significant angular dependence of the DHR, but little dependence on grain size and density. Most of the algorithms for retrieving snow surface temperatures from space (e.g., [1,12,13]) have been developed based on the simulated emissivity by Dozier and Warren [11].

Rees and James [14] investigated angular variation of the infrared emissivity of an ice surface using a simple TIR sensor for the measurement of brightness temperature averaged between 8 and 14 μm, together with a thermocouple thermometer for measuring the physical temperature of the surface. They found that the broadband emissivity of ice surfaces is in agreement with the Fresnel formula for a plane interface. Subsequently, Rees [15,16] attempted to measure the emissivity of various snow covers including fresh snow, employing the same measurement approach, yet the resulted emissivity seems to vary widely between 0.70 and 0.92, even in the same snow type (fresh snow). This is possibly due to a failure in making accurate physical temperature measurements at the feathery low-density surface of the fresh snow cover.

Salisbury *et al.* [17] conducted laboratory measurements of DHR and found that snow emissivity varies depending on snow types, including frost, fine new snow, and medium- and coarse-granular snow, and the resultant emissivity spectra deviate notably from the simulated ones based on the Mie theory. These measured emissivity spectra are the first practical emissivity spectra of snow and are archived in the ASTER spectral library [18], although obtained only for a near nadir exitance angle (10° from the normal) owing to limitations in the instrument design [17]. The snow emissivity spectra have been used for developing a recent remote-sensing algorithm to retrieve snow surface temperature from data of the moderate resolution imaging spectroradiometer (MODIS) [4].

Wald [19] proposed several theoretical approaches to simulating grain-size-dependent emissivity spectra and succeeded in modeling the spectral DHR (at the near nadir angle) of the disaggregated coarse-granular snow and welded snow obtained by Salisbury *et al.* [17]. The DHR of disaggregated snow was modeled by employing the diffraction subtraction method in which the diffracted components of the scattered light were subtracted in the RT simulation for a close-packed snow media, while the DHR of the welded snow was expressed as the weighted sum of the RT reflectance and Fresnel reflectance. Wald [19] also pointed out that the angular dependence determined with any RT approach is only applicable for disaggregated snow samples, and the emissivity of welded samples should be partly accounted for using the Fresnel reflectance theory, which itself has a strong angular dependence. Therefore, not only grain size but also cementation effects—thus whether the snow is welded or disaggregated—are considered important factors that determine the directionality of snow emissivity [in general, snow particles are expressed as "an aggregate of ice crystals." However, in this paper, we use the term "disaggregated snow (or particles)" for expressing snow conditions consisting of fine- to coarse-grained snow particles according to the usage in [19] to discriminate them from those consisted of welded film-like ice particles such as in the case of sun crust snow].

Hori *et al.* [20] conducted *in situ* measurements of the spectral directional emissivity of snow and ice and revealed that snow emissivity actually varies depending both on snow surface grain size and exitance angle. Their *in situ* measured emissivities clearly indicated that angular emissivity of snow in TIR is near isotropic for fine disaggregated snow but approaches an anisotropic nature, exhibiting specular reflectance, as snow particles become larger and more welded. Thus the results of [20] further demonstrated the importance of understanding whether snow grains are welded or not when determining the directional emissivity of snow. Hori *et al.* [20] also showed the close correlation between TIR emissivity and shortwave infrared reflectance measured for various snow types (fine, medium, coarse, and sun crust), which again indicates that TIR emissivity varies depending on the snow grain shape on the upper skin surface. They also discussed the applicability of the spectral contrast in TIR snow emissivity around the wavelengths 11–12 μm in an attempt to discriminate among snow types from space. The applicability of TIR spectral contrast to the monitoring of snow and ice from space was also examined by Tonooka and Watanabe [21] based on nadir angle spectra from the ASTER spectral library.

Cheng *et al.* [22] recently compared several RT models in order to examine their capability in simulating the *in situ* measured snow TIR emissivity acquired by [20]. They investigated RT models based on the Mie scattering theory, both with and without corrections for the packing effect, which violates the independent scattering approximation assumed in the theory. Their results indicated that several RT models based on the Mie theory with the diffraction subtraction correction proposed by [19] were able to simulate the emissivity only at the nadir angle. However, none of the models succeeded in simulating snow emissivities at off-nadir angles.

The snow surface is generally densely packed, but at the same time is sometimes porous and sometimes a specular medium and therefore has complex surface structures from the point of views of the light

scattering. Although, as described above, the emissivity of snow has been modeled by rigorous application of Mie scattering and RT theories, currently no theoretically unified model can simulate the angular dependence of emissivity spectra for different snow and ice types. There remain discrepancies between the simulated and *in situ* measured emissivities, particularly at wavelengths longer than 10.5 μm, where typical split-window channels of satellite-borne optical sensors are located. These instruments are commonly used for the remote sensing of surface temperatures from space. Approaches involving the Mie scattering and RT models therefore fail to accurately simulate TIR emissive properties of snow particles with wide ranges of sphericity and size. This problem has also been discussed in [17].

For practical applications, such as the remote sensing of snow surface temperature from space, a simple model that is capable of simulating angular and grain-size-dependent TIR emissivity spectra is desired. As Wald [19] proposed, a weighted summation of a RT model (using the diffraction subtraction method) and the Fresnel reflectance could be one potential approach to such a goal, although no such model has yet been presented.

Recent advances in handheld thermographic imaging technology has enabled and facilitated observation of *in situ* TIR emissive behaviors of snow surfaces with high spatial resolution (e.g., [23,24]). We recently carried out thermography measurements coincident with snow pit works in snowfields and gained physical insights into the TIR emissive behaviors of several different snow types. Based on these thermography measurement results in addition to the experimental knowledge obtained in the past studies, we propose, in this study, a semi-empirical model of snow surface emissivity to reproduce the *in situ* measured directional snow emissivity spectra [20]. The model introduces a weighting parameter that characterizes the specularity of the bulk snow surface and bridges the gap between the specular and blackbody-like behaviors of snow. This approach provides an alternative to inappropriate RT calculations for the densely packed snow medium.

Section 2 briefly reviews and summarizes past experimental knowledge from the literature. The thermography images of various snow types acquired *in situ* are also discussed; these images give insight into the thermal radiative behaviors of snow covers. Section 3 describes our modeling of snow emissivity, including the concept for constructing a snow emissivity model and the introduction of emissivity equations. Comparison of the model with past *in situ* measured spectra and an example of the application of the emissivity model to an analysis of thermography images are also presented. Section 4 comprises a brief discussion on the validity and applicability of the emissivity model to other uses such as remote sensing from space. A summary and conclusion of this paper is included in the Section 5.

2. Experimental Knowledge

A. Typical Emissivity Spectra Obtained in Past Experimental Studies

As described above, there is still a conflict between snow emissivity simulated by RT calculations and that measured by laboratory and *in situ* experiments. In this study, we employ the angular-dependent spectral emissivity of snow and ice measured by Hori *et al.* [20] to construct a practical model for simulating the emissive behavior of the snow surface.

Figure 1 indicates the *in situ* measured spectral emissivity of five different snow types: fine dendrite, medium-granular, coarse-grained, sun crust, and bare ice with a smooth specular surface. Each is

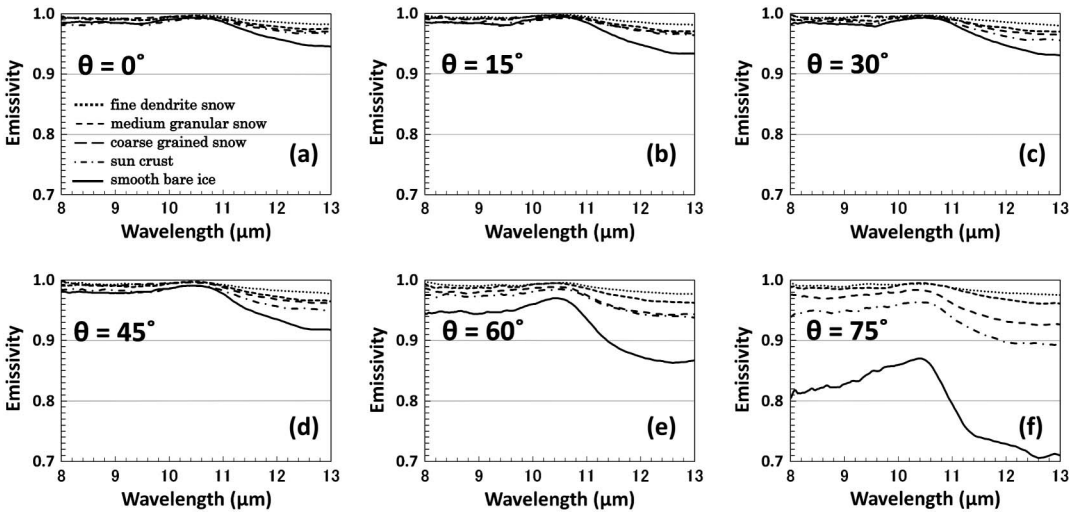

Fig. 1. *In situ* measured spectral directional emissivity of five different snow types (fine dendrite, medium-granular snow, coarse-grained snow, sun crust, and smooth bare ice) at six exitance angles (θ): (a) 0°, (b) 15°, (c) 30°, (d) 45°, (e) 60°, and (f) 75° measured from the surface normal toward the sensor [20] reproduced from the JAXA *in situ* data archive for GCOM mission [25].

shown for five different exitance angles. Typical snow emissivity spectra have a reststrahlen band (emissivity trough) centered at 13 μm, which occur at surface-scattering maxima typically associated with fundamental molecular vibration bands [26,19]. Spectra also have an emissivity peak at 10.5 μm, at which the single scattering albedo of ice particles reaches a minimum in the 8–14 μm window. As the angle of exitance increases, the emissivity at the surface-scattering maximum decreases. This angular behavior is qualitatively explained by the fact that the fraction of emission that undergoes multiple scattering inside the snow layer decreases toward the surface because of leakage from the surface, and as the exitance angle increases, the field of view at off-nadir angles incorporates a greater contribution from the smaller flux closer to the surface [26]. As snow particles age and become welded and therefore flat, the surface scattering component becomes dominant; therefore the spectra become more similar to the spectrum of a smooth ice surface (the extreme lower limit of ice emissivity), which can be completely simulated with the Fresnel reflectance theory using the complex refractive indices of ice [27]. As indicated in Fig. 1, the increase in exitance angle from 0° to 75° further enhances specular reflectances. These *in situ* measurements by [20] verified that the expected angular and snow-type dependences of snow emissivity predicted by [19] do in fact exist.

B. Insights from Thermography Images of Snow Surfaces

1. *Advantages of the Thermography for Snow Observations*

The past studies reviewed above have revealed that snow TIR emissivity is dependent on snow particle morphology and the angle of exitance. It should be noted here, however, that past *in situ* or laboratory-measured emissive properties were in all cases derived not from individual snow particles such as fine dendrite crystals or crusts, but rather for bulk snow surfaces (i.e., a mixture of ice facets and cavities between ice particles) within the field of view of the spectrometer (e.g., approx. 3–4 cm square at the nadir and over 10 cm square at off-nadir angles for measurements in [20]). Thus, the average snow emissivity for several tens of square centimeters has been evaluated, and as yet no study has captured the emissive properties of individual snow particles.

Recent technological advances in developing handheld thermography equipment have enabled us to take thermography images in a real snowfield, so the thermal emissive behavior of individual snow particles can be easily visualized *in situ*. The typical spectral range of the thermography camera is broad, around the wavelengths 7–13 μm, and thus the sensitivity to variation in snow-type-dependent emission is less than that for a high spectral resolution spectrometer such as FT-IR. However, the thermography is capable of visualizing emissive behaviors of individual ice particles, which is a significant advantage of this technology. In addition, the thermography measurements have the potential to rapidly assess the spatial uniformity of snow types in the snow cover. We performed *in situ* thermography measurements at snowfields in Hokkaido, Japan, in Feb. of 2011, 2012, and 2013 using a portable IR camera [FLIR, SC660, detector: focal plane array (uncooled microbolometer), spectral range: 7.5–13 μm, IR image resolution: 640 × 480 pixels, weight: 1.7 kg, dimensions: 299 × 144 × 147 mm, temperature range: −40 to +120°C, accuracy of absolute temperature: 2°C, temperature resolution:<0.045 K at 30°C] and gained significant physical insights into the thermal emissive behaviors of various types of snow cover and snow crystals.

2. *Appearance of Snow Cover in the Thermography*

Figure 2 shows visible image photographs of a snowfield taken in Hokkaido, Japan, during the period Feb. 24–26 in 2011. Sky conditions were mostly clear except for on Feb. 24 when it was partly cloudy at times. During the observation period, the air temperature (T_{air}) varied widely, and therefore snow type on the top surface also changed day by day. Variation in snow types are as follows: partly rounded particles and faceted particles on Feb. 24 [$T_{air} = -5$ to 0°C, snow grain size at the top surface r_{snw} (an effective ice particle radius "r_2" obtained by snow pit work expressing one-half the branch width of dendrites or one-half the dimension of the narrower portion of broken crystal [28]) = 50 to 300 μm]; granular snow (coarse-grained old snow) and patches of sun crust in the daytime of Feb. 25 ($T_{air} = 3$ to 5°C, $r_{snw} =$ 100 to 300 μm for granular particles); granular snow with small fragments of sun crust in the nighttime of Feb. 25 ($T_{air} = -8$ to −4°C, r_{snw} not available); and

Fig. 2. Visible image photographs of snow covers taken at a snowfield in Hokkaido, Japan, on (a) Feb. 24 (surface snow type: partly rounded particles and faceted particles; air temperature: −5 to 0°C), (b) daytime on Feb. 25 (granular snow and patches of sun crust, 3°C–5°C), (c) nighttime on Feb. 25 (granular snow and fragments of sun crust, −8 to −4°C), and (d) Feb. 26, 2011 (granular snow, −8 to −4°C).

granular snow on Feb. 26 (T_{air} = −8 to −4°C, r_{snw} = 100 to 400 μm for granular particles).

Although there are no discernible changes in brightness in the visible image photographs in Fig. 2, thermography images shown in Fig. 3 reveal spatial pattern changes day by day. For example, the pattern of brightness temperatures over the snow cover appears uniform when the top surface was covered with finer snow particles on Feb. 24 [Fig. 3(a)]. However, the spatial pattern transformed into a nonuniform one in the daytime on Feb. 25 [Fig. 3(b)] when the air temperature was so high as a result of the sunshine that snow grains on the surface became coarse and welded into a sun crust during the daylight hours. Because the TIR emissivity of a sun crust is lower than those of disaggregated particles as shown in Fig. 1, under a clear cold sky, the sun crust emits less radiation than the surrounding snow (granular snow in this case) and reflects much more of the downwelling cold sky radiance from its surface to the thermography camera. Thus the apparent brightness temperature of the sun crust (shown as a dark color in the image) becomes colder than that of the surrounding granular snow (shown in bright color). In the nighttime of Feb. 25, the patches of sun crust were found to be disappearing [Fig. 3(c)], possibly due to sublimation, and had mostly disappeared by the following day [Feb. 26, Fig. 3(d)].

There are also some interesting phenomena shown in Fig. 3, which are worthy of individual note: several warm spots are seen at the snow surface in the nighttime of Feb. 25 [Fig. 3(c)], and a vertical temperature gradient is seen across the snow pit wall on Feb. 26 [Fig. 3(d)]. The warm spots on Feb. 25 are actual warming of the snow cover, possibly because of the refreezing of melt water, whereas the vertical temperature change in the snow pit is a typical temperature gradient seen in the snow cover. Both images highlight the potential of thermographic imaging as a snow survey tool for applications such as snow pit work and others. Further discussion of the applications of thermography is beyond the scope of this paper.

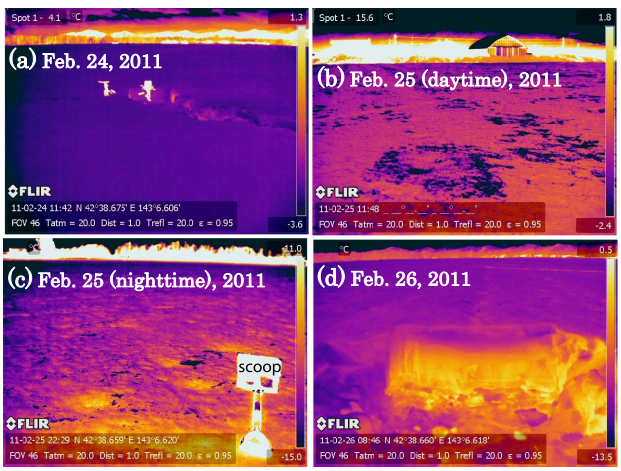

Fig. 3. Thermography images of snow covers taken at the same location and times as in Fig. 2.

The snow type dependence of apparent brightness temperatures, as seen in Fig. 3(b), is further examined below using close-up images of the sun crust, granular snow, and fine dendrite snow.

3. *Sun Crust (Ice Formations)*

The highly reflective nature of the sun crust seen in Fig. 3 can be further visualized by the close-up thermography images shown in Fig. 4, which were taken on the same date as Fig. 3 but at a shorter distance from the surface, about a few tens of centimeters. In the left image [Fig. 4(a)], the region of dark color again indicates patches of sun crust surrounded by granular snow grains shown in bright color. The right image [Fig. 4(b)] is the same snow, but with a bare hand placed just over the sun crust, so that a large TIR emission from the skin of the bare hand could be reflected at the sun crust and directed to the IR camera. The highly specular nature of the sun crust was well visualized in this example. Emissivities of the sun crust can be roughly estimated from the increased brightness temperature in Fig. 4. Considering that the temperatures of the bare hand and the sun crust are 15°C and −0.5°C, respectively, and the enhanced brightness temperatures due to the reflection of the bare hand emission are ranged around 0.1°C–1.1°C, which are inferred from the brightness temperatures of the bare hand, bulk snow area outside the sun crust, and the reflected portions of the sun crust in the IR image, emissivities of the sun crust are estimated to range around 0.935–0.965. In addition, sun crust emissivities are seen to vary depending on the location within the ice plate of sun crust. The estimated emissivities of the sun crust are consistent with or somewhat lower than the past *in situ* measured spectra at slanted exitance angles of around 45° to 60°, which indicates that, depending on the specularity on the sun crust, the emissivity of sun crust can be further lower than that shown in Fig. 1. Finally, under clear skies, a welded snow particle such as the sun crust itself is efficient at reflecting the downwelling cold sky radiance. Thus the existence of a sun crust can be easily identified by thermography.

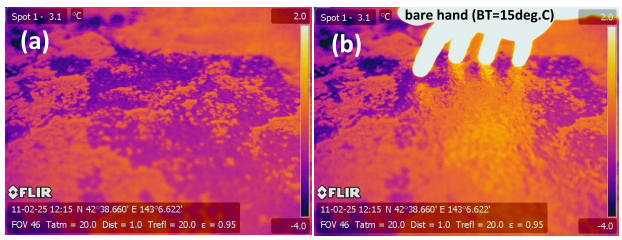

Fig. 4. Close-up thermography images of sun crust snow taken at the snowfield in Hokkaido, Japan, on Feb. 25 (daytime), 2011: (a) without and (b) with a bare hand laid over the snow surface. In (b) the specular reflection of TIR emission from the warm bare hand can be seen to occur at the sun crust surface.

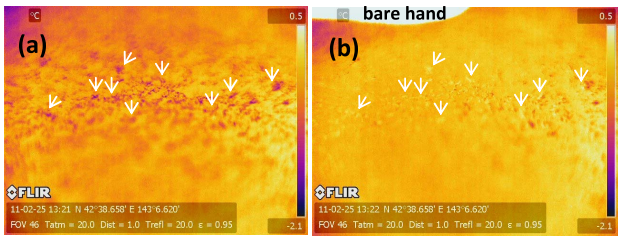

Fig. 5. Close-up thermography images of granular snow particles taken at the snowfield in Hokkaido, Japan, on Feb. 25, 2011: (a) without and (b) with a bare hand laid over the snow surface. In (b) the specular reflection of TIR emission from the warm bare hand can be seen to occur at the upper surface of granular crystal facets, shown as bright spots indicated with white arrows.

4. *Granular Snow Particles (Melt Forms)*

Granular snow particles are defined as "clustered rounded grains" in the "melt forms" class in the international classification of snow crystals [29]. IR images in Fig. 5 were obtained at the surface, just next to the sun crust area shown in Fig. 4, on the same date at a much shorter distance, ~10 cm from the surface. In the left image, granular ice particles located in the top skin surface appear darker (colder) than the surrounding warm areas, which consist of interstitial microcavities between individual granular ice particles. At a glance, it seems that the darkness of the granular particles is only due to radiative cooling of the ice particle itself. However, when a bare hand is laid over the surface, as shown in the right image, strong TIR radiation from the hand was clearly seen to be reflected from the upper facets of the granular ice particles [the dark spots in Fig. 5(a) turn into bright ones in Fig. 5(b)], while the TIR radiation from the bare hand seems to not affect the brightness of the surrounding cavity spaces. The interstitial cavities individually form tiny holes surrounded by granular ice particles and, therefore, on the whole are expected to behave like a blackbody surface that radiates isotropic thermal emission upward. As a result, the interstitial cavities are considered to exhibit a negligibly reflective nature.

5. *Fine Dendrite Snow (Precipitation Particles)*

Our final example of close-up IR images of fresh fine snow particles partly consisting of dendrite crystals are shown in Fig. 6; these images were captured on Feb. 7, 2013, at Hokkaido, Japan. In the case of fresh snow, the heat capacity of snow particles in the top skin surface layer is so low that a bare hand laid over the snow cover heats up the bulk surface without exhibiting overall reflectivity, as shown in Fig. 6(b). However, several (but not all) dendrite crystals, like those shown in Fig. 6(c), which were scattered across the surface and appear dark in Fig. 6(a), become bright hot spots in Fig. 6(b). This phenomenon again indicates that even a new fine snow particle with flat crystal facets can have a highly (specular) TIR reflective nature. However, because the dendrite crystals are oriented randomly on the surface, not all of

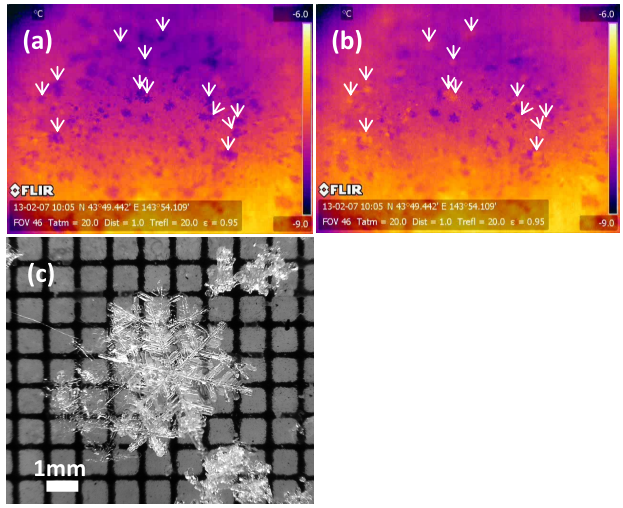

Fig. 6. Close-up thermography images of fine dendrite snow taken at a snowfield in Hokkaido, Japan, on Feb. 7, 2013: (a) without and (b) with a bare hand laid over the snow surface. (c) A microphotograph of dendrite crystals taken at the snow surface. In (b) the specular reflection of TIR emission from the warm bare hand can be seen to occur at several dendrite crystal facets, shown as bright spots indicated with white arrows.

the particles are seen to exhibit bright reflection simultaneously. Rather, the location of the hot spots moves to different crystals as the bare hand swings over the surface (not shown in the figures). These observed emissive behaviors of the snow surface imply that (1) individual dendrite crystals themselves have flat facets that exhibit low emissivity and high specular reflectance, (2) the poor emissive nature of the dendrite crystal (i.e., being a hot spot) cannot be observed for all particles from a single fixed viewing angle, and (3) on average the emissivity of a bulk surface consisting of dendrite crystals can be determined by a combination of the specular reflective nature of randomly oriented dendrite crystals and the isotropic emissive nature of interstitial cavities on the surface.

6. *An Extracted Concept for Modeling the Emissive Behaviors of Snow Cover*

The observed thermal emissive behaviors of snow particles illustrated above brought a new physical insight: that the microscopic but flat facet of an individual ice particle is considered to have the same emissive or reflective properties as a specular surface with Fresnel reflectance, whatever the snow type is, whereas the interstitial cavities behave like a blackbody. Therefore, the emissive nature of a bulk snow surface can be expressed as a mixture of the two components: the specular and blackbody fractions. The concept of this emissive behavior is illustrated in Fig. 7. The emissivity of the bulk snow surface varies as a function of the effective areal fraction (f_{sp}) of flat crystal facets or plates with specular reflectance within the bulk surface. At the same time, the emissivity of the specular fraction itself also varies

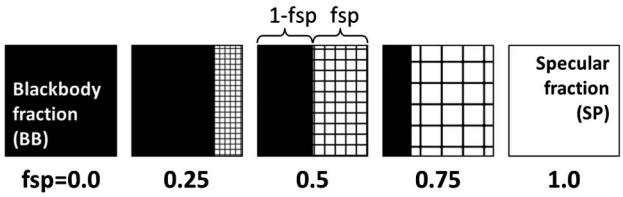

Fig. 7. Conceptual illustration of a two component surface model for reproducing the *in situ* measured emissivity of snow and ice. The two components consist of a surface behaving like blackbody (BB) and a specular surface (SP), both of which are related via an effective areal fraction of the specular component (f_{sp}) within a unit of surface area. As the f_{sp} changes, the emissivity of the latter SP component itself is assumed to vary, from the emissivity of a horizontal icy mirror predicted by the Fresnel reflectance theory (when $f_{sp} = 1.0$), to that of a mixture of randomly oriented ice particles with specular facets and the horizontal mirror (when f_{sp} is smaller than 1.0). The emissivity of BB is always constant (i.e., 1.0).

as the f_{sp} changes, which is inferred from the fact that the effective angular orientation of particle facets or plates changes from nearly normal in smooth sun crusts or bare ice, to random in the case of dendrite crystals.

As a result of these phenomena, emissive behaviors of snow cover vary between blackbody-like and fully specular, depending on the snow particle type and therefore the specularity of the bulk surface, which is illustrated in Fig. 8. The definitions of snow grain shape are described in Fig. 8, based both on the Japanese Society of Snow and Ice [30] and the international classification in [29]. A perfectly smooth flat surface such as the bare ice shown on the right side of Fig. 8 exhibits specular-type reflectivity and emissive properties, which are fully modeled by the Fresnel reflectance theory. As snow particles become finer and more disaggregated, the surface becomes rough and the areal fraction of specular facets within the bulk snow surface is reduced. In turn, tiny interstitial cavities surrounding the specular particles (ice crystals) become an effective near-isotropic radiator, shown in the middle of Fig. 8. In an extreme case, a bulk snow surface consisting solely of fine precipitation particles no longer exhibits an anisotropic reflective nature, but comes to radiate an ideal isotropic emission close to blackbody emission (left side in Fig. 8), as also inferred from Figs. 1 and 6.

3. Modeling of Snow Emissivity

A. Emissivity Model

Based on past experimental measurements and the physical insights gained from the thermography measurements of this study, we construct a simple semi-empirical model to characterize the spectral directional emissivity of a snow surface with various grain sizes and crystal types and compare the model with the past *in situ* measured spectra acquired by [20].

We assume that the angular-dependent emissivity of snow cover $\varepsilon_{snow}(\lambda, \theta)$ can be basically expressed by a linear combination of the isotropic blackbody component ($\varepsilon_{bb}(\lambda) = 1$) and an apparent

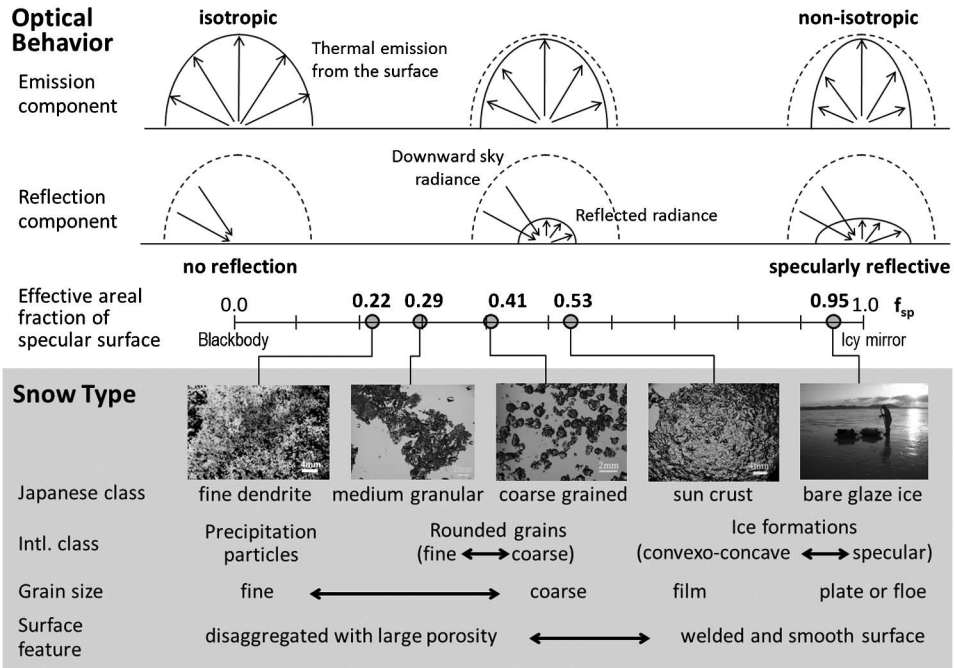

Fig. 8. Conceptual illustration of the emissive behaviors of snow in the TIR wavelength region. Snow types are shown both for the Japanese classification [30] and international classification of snow type [29]. Also shown are the values of an effective areal fraction of specular surface (f_{sp}) determined for individual snow types by comparing the modeled emissivity spectra with the *in situ* measured spectra in Fig. 10.

emissivity of the specular fraction ($\varepsilon_{\mathrm{sp\_app}}(\lambda,\theta)$), employing a weighting parameter that characterizes the specularity of the snow surface as follows:

$$\varepsilon_{\mathrm{snow}}(\lambda,\theta) = \varepsilon_{\mathrm{bb}}(\lambda)(1-f_{\mathrm{sp}}) + \varepsilon_{\mathrm{sp\_app}}(\lambda,\theta)f_{\mathrm{sp}}, \quad (1)$$

where λ is the wavelength, θ is the angle of exitance measured from the normal, and f_{sp} is the weighting parameter, indicating an effective areal fraction of specular surface within the bulk surface. In this model we consider that the apparent emissivity of the specular surface $\varepsilon_{\mathrm{sp\_app}}(\lambda,\theta)$ itself also varies as the specular portion f_{sp} changes, as explained in Fig. 7; this is expressed by the following equation:

$$\varepsilon_{\mathrm{sp\_app}}(\lambda,\theta) = \varepsilon_{\mathrm{sp}}(\lambda,45°)(1-f_{\mathrm{sp}}) + \varepsilon_{\mathrm{sp}}(\lambda,\theta)f_{\mathrm{sp}}, \quad (2)$$

where $\varepsilon_{\mathrm{sp}}(\lambda,\theta)$ is the emissivity of an ideal smooth ice surface simulated with the Fresnel reflectance $\rho_{\mathrm{sp}}(\lambda,\theta)$ by Kirchhoff's law $\varepsilon_{\mathrm{sp}}(\lambda,\theta) = 1-\rho_{\mathrm{sp}}(\lambda,\theta)$ [26].

In Eq. (2) we assume that the apparent emissivity of the specular portion $\varepsilon_{\mathrm{sp\_app}}(\lambda,\theta)$ can be expressed as a weighted sum of the emissivity of randomly oriented specular ice particles with an effective orientation angle of 45° and that of a horizontal specular ice plate. The physical implication of this assumption can be interpreted as follows. When the snow surface consists of only specular ice plate or pieces if disaggregated (i.e., f_{sp} is large, as in the cases of smooth bare ice or a welded sun crust), then the specular ice surface tends to orient upward (the normal angle is perpendicular to the horizontal bulk surface) and their apparent specular emissivity is identical to the ideal Fresnel reflectance $\varepsilon_{\mathrm{sp}}(\lambda,\theta)$. In contrast, as snow particles become more finely disaggregated (as f_{sp} is becoming smaller as in the cases of fine, medium, and coarse-grained snow), the bulk snow surface becomes a porous medium comprising ensembles of randomly oriented ice particles with specular crystal facets. Thus, the apparent emissivity of the specular portion $\varepsilon_{\mathrm{sp\_app}}(\lambda,\theta)$ is thought to approach the specular emissivity at an effective orientation (i.e., exitance) angle of 45° measured from the direction of the line of sight at the lower limit of f_{sp}.

With these assumptions regarding the TIR emissive behavior of snow particles, we can determine the spectral directional emissivity of a snow surface uniquely by identifying f_{sp}, which can subsequently be translated into information on snow grain size or snow type. This approach will enable and facilitate remote sensing of the specular fraction of snow (i.e., a measure of snow type or grain size) by making use of the spectral contrast of snow emissivity at wavelengths of between 11 and 12 μm [20]. This is briefly discussed below in Section 4.

Figure 9 illustrates the simulated spectral directional emissivity of snow using the semi-empirical model [Eq. (1) and Eq. (2)] for various exitance angles between 0° and 80°, with the weighting of f_{sp} around 0.2–1.0. The simulated spectra captured well the features of snow emissivity at TIR wavelengths. For example, as the exitance angle increases, the emissivity smoothly decreases, particularly at wavelengths longer than 10.5 μm, owing to the enhancement of reflection in the reststrahlen band. In addition, as f_{sp} increases, the spectra decrease in phase and then asymptotically approach those simulated by the Fresnel reflectance theory, such as that where $f_{\mathrm{sp}} = 1.0$ (Fig. 9(e)).

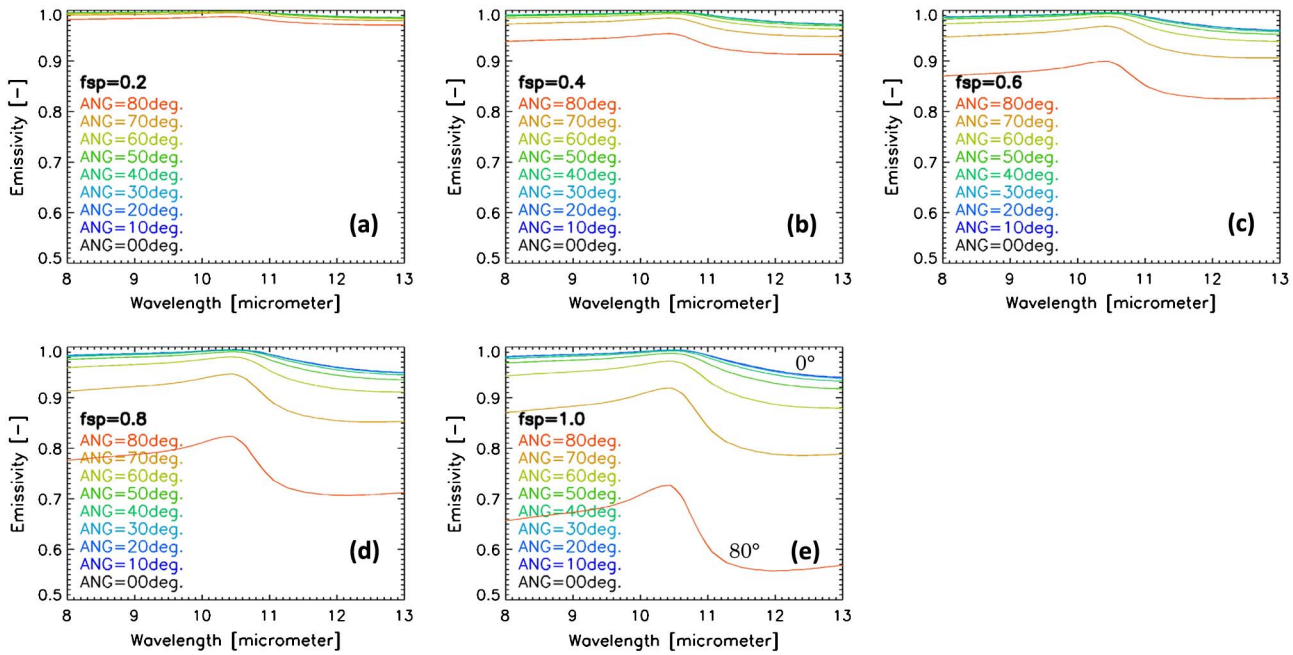

Fig. 9. Simulated spectral directional emissivity using the semi-empirical model with the weighting parameters of (a) $f_{\mathrm{sp}} = 0.2$, (b) $f_{\mathrm{sp}} = 0.4$, (c) $f_{\mathrm{sp}} = 0.6$, (d) $f_{\mathrm{sp}} = 0.8$, and (e) $f_{\mathrm{sp}} = 1.0$, as a function of exitance angles (ANG) between 0° and 80°.

B. Comparison with *In Situ* Measurements

The degree to which the modeled emissivity spectra can reproduce the *in situ* measured spectra is shown in Fig. 10 and Table 1. The reproduced emissivity spectra were simulated using the f_{sp} indicated for individual snow types shown in the figures and are plotted as circle symbols over the *in situ* measured spectra by solid lines obtained for six exitance angles: 0°, 15°, 30°, 45°, 60°, and 75°. The f_{sp} for each snow type were determined using the simulated directional spectra of all exitance angles, so that the RMSE of the simulated spectra is at a minimum for the wavelength range 8.0–13.0 μm. RMSE values evaluated for each angle and for narrower wavelength ranges 8.0–10.5 μm and 10.5–13.0 μm (the latter range covers the split-window spectral channels of MODIS ch31 and 32) are also shown together with the overall RMSE values in Table 1. It is important to note that the *in situ* measured emissivity spectra in the shorter wavelength range around 8–10 μm are somewhat variable and may be affected by measurement errors due to self-emission from the spectrometer [20] as also shown in Fig. 10.

As shown in Table 1 the overall RMSE evaluated for the entire wavelength range are less than 0.008 for all snow types, although the RMSE evaluated for individual angle cases can be worse up to 0.012 and 0.0093 for coarse-grained snow at 60° and 75° and 0.014 and 0.0099 for bare ice at 60° and 75°. The spectral deviations in the worse cases are both positive and negative as shown in Fig. 10 and are considered to partly originate from measurement errors due to the spatial heterogeneity of snow type possibly encountered in the *in situ* observations. Because the fore-optics of the spectrometer used by [20] cannot be directed at exactly the same area of the snow surface for different exitance angle measurements [31], the instrument may observe slightly different areal fraction of snow types.

The RMSE evaluated for the narrower half-wavelength ranges exhibit variations similar to the overall values with slightly higher RMSE values, e.g., 0.012 and 0.016 for coarse-grained snow and 0.018 (worst case in this study) and 0.012 for bare ice. As the past study [22] revealed, the theoretical RT models overestimate the snow emissivities at large exitance angles. For example, even a best RT model in [22] exhibits RMSE ranges over 0.023–0.029 for the coarse-grained snow and 0.024–0.058 for the sun crust case at exitance angles 60°–75° estimated for a slightly longer wavelength range 11–13 μm. Even if the difference of the wavelength range is taken into account, the spectral deviations of the RT simulations are significantly larger than our results and biased. Thus the simulated spectra of this study are considered to capture well the overall features of the snow emissivity spectra; that is, the angular and grain size dependences, with possible uncertainties in emissivity less than 0.01 in most cases, which indicates the high potential of the semi-empirical emissivity model for simulating the directional emissivity of snow with various grain sizes.

As a result, the weighting parameter f_{sp} determined in the simulation can be interpreted as a measure of snow grain type as follows: $f_{sp} = 0.22$, fine

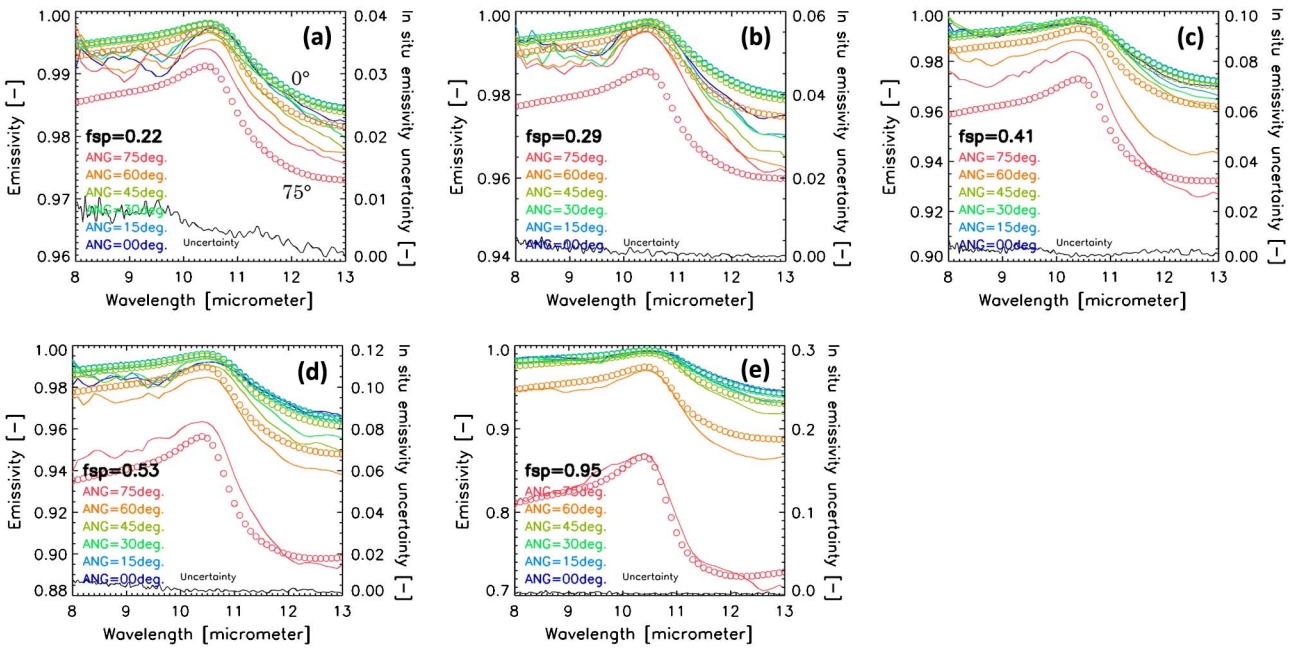

Fig. 10. Comparison between the simulated spectral directional emissivity (circle symbols) with *in situ* measured ones (solid lines) for (a) fine dendrite snow, (b) medium granular snow, (c) coarse grained snow, (d) sun crust, and (e) smooth bare ice, shown for six exitance angles (ANG) of 0, 15, 30, 45, 60, and 75°. The weighting parameters f_{sp} were determined so that RMSE of the simulated spectra for all exitance angles is at a minimum. Also shown as a thin solid line around the bottom of each figure is the uncertainty of the *in situ* measured emissivity due to the instrument self-emission [20].

Table 1. Determined f_{sp} and RMSE of the Simulated Emissivity Spectra using the Semi-Empirical Model

		λ: 8–13 μm		λ: 8–10.5 μm	λ: 10.5–13 μm
Snow Type	Exitance Angle (deg.)	f_{sp}	RMSE	RMSE	RMSE
Fine dendrite snow	0–75	0.22	0.0030	0.0032	0.0028
	0		0.0030	0.0040	0.0013
	15		0.0022	0.0023	0.0020
	30		0.0022	0.0021	0.0022
	45		0.0029	0.0022	0.0034
	60		0.0030	0.0029	0.0031
	75		0.0043	0.0047	0.0038
Medium granular snow	0–75	0.29	0.0062	0.0046	0.0074
	0		0.0038	0.0033	0.0043
	15		0.0051	0.0030	0.0065
	30		0.0062	0.0051	0.0071
	45		0.0066	0.0030	0.0088
	60		0.0064	0.0032	0.0083
	75		0.0081	0.0080	0.0082
Coarse-grained snow	0–75	0.41	0.0067	0.0054	0.0078
	0		0.0020	0.0016	0.0023
	15		0.0029	0.0014	0.0039
	30		0.0040	0.0019	0.0052
	45		0.0045	0.0025	0.0057
	60		0.0117	0.0051	0.0156
	75		0.0093	0.0116	0.0065
Sun crust	0–75	0.53	0.0066	0.0069	0.0064
	0		0.0052	0.0072	0.0018
	15		0.0048	0.0066	0.0015
	30		0.0063	0.0050	0.0074
	45		0.0078	0.0065	0.0089
	60		0.0066	0.0062	0.0070
	75		0.0083	0.0089	0.0077
Bare ice	0–75	0.95	0.0080	0.0050	0.0101
	0		0.0023	0.0024	0.0021
	15		0.0053	0.0034	0.0067
	30		0.0053	0.0039	0.0063
	45		0.0061	0.0023	0.0082
	60		0.0138	0.0076	0.0178
	75		0.0099	0.0072	0.0119

dendrite snow; $f_{sp} = 0.29$, medium granular snow; $f_{sp} = 0.41$, coarse-grained snow; $f_{sp} = 0.53$, sun crust; and $f_{sp} = 0.95$, bare ice with a smooth surface. These are also indicated on the f_{sp} scale in Fig. 8. From the comparison between determined f_{sp} and the photographs of ice crystals in Fig. 8, it can be seen that most disaggregated snow types, such as fine to coarse-grained snow, have an f_{sp} less than 0.5, and that f_{sp} becomes smaller, up to around 0.2, as the grain size decreases. Welded snow of a sun crust and smooth ice plate can have f_{sp} over 0.5, up to 1.0, depending on the extent to which the ice particles are connected together, filling the interstitial cavities and how flat and specular the ice surface becomes.

C. An Application Example: Simulation of Possible Temperature Bias in Thermography Image

As an example of the application of the semi-empirical emissivity model constructed in this study, it was used to estimate possible temperature bias in measurements made with a thermography camera, taking into account relative spectral response.

Figure 11 indicates the estimated possible negative temperature bias in the thermography images taken with FLIR SC640 with the setting of target emissivity of 1.0 (i.e., assumption of blackbody behavior). The bias simulations were performed using individual f_{sp} values identified for the typical five snow types shown in Fig. 10. In this simulation, the spectral response curve for the FLIR SC640 instrument provided by FLIR Systems, Inc. was used. In addition, for simplicity, downward atmospheric emission that could be reflected at the snow surface and directed to the thermographic imager is neglected, simulating conditions similar to clear cold skies.

As shown in Fig. 11, the temperature bias has a tendency to decrease as the surface temperature decreases, which results from the nonlinear response of the Planck radiance to absolute temperature.

The simulated temperature bias exhibits explicit dependences on snow grain size and exitance (viewing) angle, despite the fact that, as mentioned previously, the thermography camera has a broader spectral response and thus has a reduced sensitivity

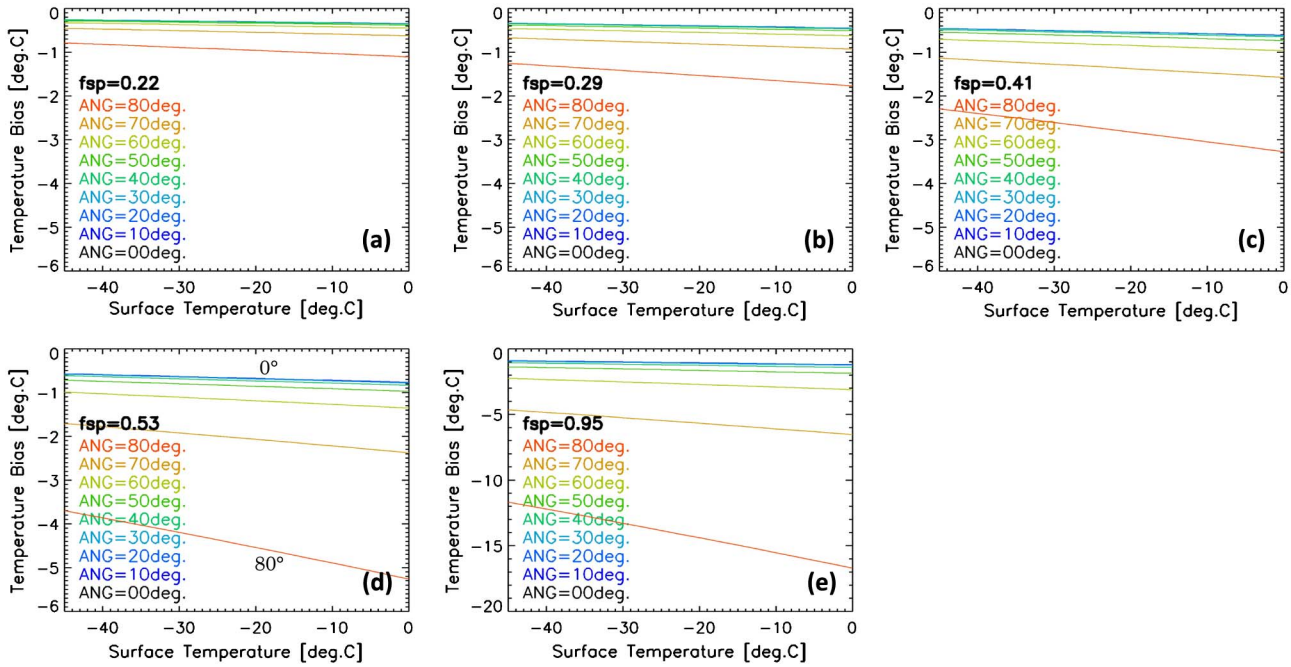

Fig. 11. Possible temperature biases in thermography image estimated for nine exitance angles (ANG) and the five weighting parameters (f_{sp}) indicated in the figures, all simulated for the FLIR SC640 spectral response. The selected weighting parameters correspond to the five typical snow types investigated by Hori *et al.* [20]: (a) $f_{sp} = 0.22$ for fine dendrite snow, (b) $f_{sp} = 0.30$ for medium granular snow, (c) $f_{sp} = 0.43$ for coarse-grained snow, (d) $f_{sp} = 0.53$ for sun crust, and (e) $f_{sp} = 0.96$ for smooth bare ice. Note that the vertical axis scale for (e) is different from the others.

to the grain size dependent emissivity variation, compared to the FT-IR spectrometer. For example, as snow grain size increases, the negative bias can increase to −0.3 to −0.4°C for fine snow, −0.4 to −0.5°C for medium granular snow, −0.6 to −0.7°C for coarse-grained snow, −0.7 to −0.8°C for sun crust, and −1.2 to −1.4°C for bare ice when the surface temperature ranges between −5 and 0°C and the viewing angle ranges between the nadir and 40°.

Considering possible angular dependence, the temperature bias does not appear to change greatly at near-nadir viewing angles smaller than 40° for all snow types; the difference from the nadir case is less than 0.5°C. However, the biases are significantly increased when the viewing angle is larger than 50° because the specular nature of the surface becomes dominant. For example, at the slanted viewing angle of 70°–80°, the negative bias can be as large as −2 to −3°C for coarse-grained and sun-crust snow, and even larger than −10°C in the extreme case of specular bare ice.

Considering these results, a temperature bias of the order of a few to 10°C should be taken into account as a possible error when measuring the surface temperature of old staged snow using thermography with a fixed setting of target emissivity. From an alternative viewpoint, however, the temperature bias could be used for discrimination of snow type when the brightness temperature of the surface exhibits a spatial nonuniformity, as already seen in the examples in Fig. 3.

4. Discussion

As mentioned in the introduction, past studies have attempted to simulate the TIR thermal behavior of snow using the Mie scattering theory [11,22] with or without correctional approaches, such as diffraction subtraction by [19]. However, these theoretically derived emissivities were found to not fully follow the directional spectra derived *in situ* (acquired by [20]) and thus cannot completely explain the snow type and exitance angle dependences.

The consistency of our modeled spectra with *in-situ*-derived directional spectra shown in Fig. 10 clearly indicates that the semi-empirical model of snow emissivity captures well the overall spectral features of TIR radiative properties of snow surfaces with various snow types and at differing exitance angles. Therefore, the approach of combining the TIR emissive properties of snow with blackbody emissivity and those of a specular surface is considered to provide the best estimates of snow emissivity at the present.

From these results, together with the insights gained from the thermography images, it is reasonable to suppose that (1) facets of individual ice particles have essentially the same emissive properties as a flat ice plate, (2) the surface structure of bulk snow changes drastically from a porous medium in the case of disaggregated fine snow, to a welded and specular one, in the case of a sun crust and bare ice, and (3) emissive properties of bulk snow are therefore determined with an effective areal fraction of the icy mirror facets or plates within a unit area of

the bulk surface (that is, f_{sp} employed in this study). Our model simply mimics the thermal emissive behavior of the bulk snow surface as it changes from a porous medium to a specular one. The model has a quite simple form but sufficient capability to reproduce the emissivity variations as functions of snow grain size and exitance angle and can therefore contribute to improving the accuracy of snow surface temperature retrieval.

For example, the model enables us to reduce unknowns when determining surface temperature and emissivity from remotely sensed radiance data because the semi-empirical model of snow emissivity is parameterized only by the f_{sp} value. In general, TIR radiance is a function of surface temperature and emissivity, and the emissivity is also a function of wavelength. Thus, even if radiances at multiple wavelengths (e.g., at two channels) are measured, the number of unknowns (temperature + emissivities at the two channels) becomes always larger than that of measured values (radiances at the two channels). The f_{sp} can relate the emissivities at different wavelengths and thus the number of unknowns are reduced to the same number as the measurements and then the problem can be solved (i.e., the surface temperature and the f_{sp} can be determined). For this purpose, the characteristic spectral contrast seen in the wavelength region 11–12 μm is suitable.

As another application of the semi-empirical model, the f_{sp} could be further translated into snow type. As shown in Fig. 8, this study confirmed the validity of the relationship between snow type and f_{sp} for the typical five different snow types. These five snow types represent various stages of snow cover evolution at dry (i.e., not wet) conditions except for the case of surface hoar (frost) which has not been measured *in situ* in the past. Thus, the "f_{sp}-snow type" relationship is considered to hold true for any snow covers as far as the types of snow is identical to one of the five types or intermediate of two types among those five types. The range of these snow types can cover most of snow conditions except for the cases of surface hoar and wet snow. Therefore, except for these two cases, we can conclude that the semi-empirical model (and the relationship between snow type and f_{sp}) holds true for most of snow covers and thus the employment of the semi-empirical model in remote sensing applications is expected to have a potential to discriminate several snow types using TIR spectroradiometer data. For this purpose, it will be necessary to examine the uncertainty in the f_{sp} determination originated from the emissivity uncertainties in the semi-empirical model (of the order of 0.01 or less as estimated above). For more precise discrimination of surface types from space, it is also desirable to conduct further validation studies to examine the applicable range of the semi-empirical model for various snow types including other types of snow, such as surface hoar (frost) and wet snow.

Finally, once the f_{sp} is retrieved, directional emissivity of the snow surface can be determined for all exitance angles, which could then be used as an indispensable boundary condition for estimating thermal emissive properties of the ground surface for polar night cloud detection, or for estimating the radiation budget over ice sheets, among others. We will further explore the possible applications of our snow emissivity model in future studies.

5. Summary and Conclusion

A semi-empirical model of angular-dependent snow emissivity spectra in TIR was constructed based on past *in situ* measured emissivity spectra and physical insights gained from the thermographic measurements of snow surfaces with various snow particle types.

Thermal emissive behaviors of individual snow particles observed by thermography were found to be essentially identical to that of a specular ice plate. The isotropic nature of the bulk surface emissivities for disaggregated snow, seen in the past *in situ* measurements, was thereby considered attributable to the porous structure of the snow surface, behaving like a blackbody, whereas welded snow simply exhibited specular behavior.

The semi-empirical model was designed to reproduce the spectral features of the *in situ* measured directional emissivities, which exhibit strong snow grain size and exitance angle dependences. Briefly, the surface exhibits blackbody-like isotropic emissive behavior when snow particles are fine and disaggregated, whereas the emissivity of the surface approaches that of a specular surface when the snow particles are welded. The degree to which the surface behaves isotropically or specularly is considered dependent on an effective areal fraction of the specular portion within a unit area of bulk snow surface (f_{sp}).

The simulated emissivity from the semi-empirical model is consistent with past *in situ* measured directional emissivity spectra for five different snow types: fine, medium, coarse-grained snow, sun crust, and specular bare ice, not only at the normal exitance angle but also at off-nadir angles up to 75°.

The consistency between the emissivity model and the *in situ* measurements indicates that it is reasonable to consider that at TIR wavelengths the snow surface is a porous medium behaving like a blackbody when finer disaggregated particles dominate, while snow behaves like an icy mirror surface when snow particles grow larger and become welded and specular plates.

The proposed semi-empirical model of snow emissivity spectra, by its simple but robust treatment of the angular, spectral, and snow type dependences with only one weighting parameter f_{sp}, facilitates the use of snow emissivity in a wide range of applications. For example, the emissivity model can be used to estimate possible errors in a broadband thermometer. The emissivity model also enables us to determine snow surface temperature and snow type

(via its emissivity) simultaneously from space using data from satellite-borne optical sensors. Further examples of the application of this model include contribution to enhancement of the accuracy of polar night cloud detection and estimation of outgoing long-wave radiation over the ice sheet. These applications would contribute to our further understanding of the TIR emissive nature of snow and ice covers in the cryosphere and thus their ongoing role in the earth's changing climate system.

References

1. J. Key and M. Haefliger, "Arctic ice surface temperature retrieval from AVHRR thermal channels," J. Geophys. Res. **97**, 5885–5893 (1992).
2. Z. Wan, "MODIS land-surface temperature algorithm theoretical basis document (LST ATBD)," Version 3.3. Contract Number NAS5-31370 (1999), available at http://modis.gsfc.nasa.gov/data/atbd/atbd_mod11.pdf.
3. S. G. Warren, "Optical properties of snow," Rev. Geophys. Space Phys. **20**, 67–89 (1982).
4. D. K. Hall, J. E. Box, K. A. Casey, S. J. Hook, C. A. Shuman, and K. Steffen, "Comparison of satellite-derived and *in situ* observations of ice and snow surface temperatures over Greenland," Remote Sens. Environ. **112**, 3739–3749 (2008).
5. Z.-L. Li, H. Wu, N. Wang, S. Qiu, S. A. Sobrino, Z. Wan, B.-H. Tang, and G. Yan, "Land surface emissivity retrieval from satellite data," Int. J. Remote Sens. **34**, 3084–3127 (2013).
6. T. Yamanouchi, K. Suzuki, and S. Kawaguchi, "Detection of clouds in Antarctica from infrared multispectral data of AVHRR," J. Meteorol. Soc. Jpn. **65**, 949–962 (1987).
7. Y. Liu, J. R. Key, R. A. Frey, S. A. Ackerman, and W. P. Menzel, "Nighttime polar cloud detection with MODIS," Remote Sens. Environ. **92**, 181–194 (2004).
8. A. C. Wilber, D. P. Kratz, and S. K. Gupta, "Surface emissivity maps for use in satellite retrievals of long-wave radiation," NASA Tech. Rep., 1999-209362 35 (1999).
9. R. Morishima, S. G. Edgington, and L. Spilker, "Regolith grain sizes of Saturn's rings inferred from Cassini–CIRS far-infrared spectra," Icarus **221**, 888–899 (2012).
10. R. H. Berger, "Snowpack optical properties in the infrared," CRREL Rep. 79 (U. S. Army Cold Regions Research and Engineering Laboratory, Hanover, New Hampshire, 1979), pp. 11.
11. J. Dozier and S. Warren, "Effect of viewing angle on the infrared brightness temperature of snow," Water Resour. Res. **18**, 1424–1434 (1982).
12. J. R. Key, J. B. Collins, C. Fowler, and R. S. Stone, "High-latitude surface temperature estimates from thermal satellite data," Remote Sens. Environ. **61**, 302–309 (1997).
13. W.-C. Snyder, Z. Wan, Y. Zhang, and Y.-Z. Feng, "Classification-based emissivity for land surface temperature measurement from space," Int. J. Remote Sens. **19**, 2753–2774 (1998).
14. W. G. Rees and S. P. James, "Angular variation of the infrared emissivity of ice and water surfaces," Int. J. Remote Sens. **13**, 2873–2886 (1992).
15. W. G. Rees, "Infrared emissivities of Arctic land cover types," Int. J. Remote Sens. **14**, 1013–1017 (1993).
16. W. G. Rees, "Infrared emissivity of Arctic winter snow," Int. J. Remote Sens. **14**, 3069–3073 (1993).
17. J. W. Salisbury, D. M. D'Aria, and A. Wald, "Measurements of thermal infrared spectral reflectance of frost, snow, and ice," J. Geophys. Res. **99**, 24235–24240 (1994).
18. ASTER Spectral Library: reproduced from the ASTER Spectral Library through the courtesy of the Jet Propulsion Laboratory, California Institute of Technology, Pasadena, California (1999), http://speclib.jpl.nasa.gov.
19. A. Wald, "Modeling thermal infrared (2–14 μm) reflectance spectra of frost and snow," J. Geophys. Res. **99**, 24241–24250 (1994).
20. M. Hori, Te. Aoki, T. Tanikawa, H. Motoyoshi, A. Hachikubo, K. Sugiura, T. Yasunari, H. Eide, R. Storvold, Y. Nakajima, and F. Takahashi, "*In situ* measured spectral directional emissivity of snow and ice in the 8–14 μm atmospheric window," Remote Sens. Environ. **100**, 486–502 (2006).
21. H. Tonooka and A. Watanabe, "Applicability of thermal infrared surface emissivity ratio for snow/ice monitoring," Proc. SPIE **5655**, 282–290 (2005).
22. J. Cheng, S. Liang, F. Weng, J. Wang, and X. Li, "Comparison of radiative transfer models for simulating snow surface thermal infrared emissivity," IEEE J. Sel. Topics Appl. Earth Observations Remote Sens. **3**, 323–336 (2010).
23. C. Shea and B. Jamieson, "Some fundamentals of handheld snow surface thermography," The Cryosphere **5**, 55–66 (2011).
24. J. Light, S. Parthasarathy, and W. Mclver, "Monitoring winter ice conditions using thermal imaging cameras equipped with infrared microbolometer sensors," Procedia Comput. Sci. **10**, 1158–1165 (2012).
25. JAXA *in situ* data archive for GCOM mission: reproduced from the archived *in-situ* data provided by Japan Aerospace Exploration Agency. http://suzaku.eorc.jaxa.jp/GCOM_C/insitu/index.html (2012).
26. B. Hapke, *Theory of Reflectance and Emittance Spectroscopy* (Cambridge University, 1993).
27. S. G. Warren, "Optical constants of ice from the ultraviolet to the microwave," Appl. Opt. **23**, 1206–1225 (1984).
28. T. Aoki, T. Aoki, M. Fukabori, A. Hachikubo, Y. Tachibana, and F. Nishio, "Effects of snow physical parameters on spectral albedo and bidirectional reflectance of snow surface," J. Geophys. Res. **105**, 10219–10236 (2000).
29. C. Fierz, R. L. Armstrong, Y. Durand, P. Etchevers, E. Greene, D. M. McClung, K. Nishimura, P. K. Satyawali, and S. A. Sokratov, "The international classification for seasonal snow on the ground," IHP-VII Technical Documents in Hydrology N°83, IACS Contribution N°1, UNESCO-IHP, Paris (2009).
30. Japanese Society of Snow and Ice, "JSSI classification for snow cover," J. Jpn. Soc. Snow Ice **60**, 419–436 (1998).
31. A. R. Korb, P. Dybwad, W. Wadsworth, and J. W. Salisbury, "Portable Fourier transform infrared spectroradiometer for field measurements of radiance and emissivity," Appl. Opt. **35**, 1679–1692 (1996).